



Remote sensing linear trends of the Gulf Stream from 1993 to 2016

Wen-Zhou Zhang^{1,2,3} · Fei Chai^{2,4} · Huijie Xue⁴ · Lie-Yauw Oey⁵

Received: 11 December 2019 / Accepted: 13 February 2020 / Published online: 5 March 2020
© Springer-Verlag GmbH Germany, part of Springer Nature 2020

Abstract

The Gulf Stream (GS) transports a massive amount of heat northward to high latitudes and releases sensible and latent heat to the atmosphere, playing an important role in the North Atlantic and European climate change. The change trends of the GS transport and pathway are still uncertain to date. Our analyses of altimeter observations from 1993 to 2016 indicate that the linear trends in surface maximum speed, transport, and latitudinal location of the GS are significant east of 61° W at the 95% level while they are small and not significant between 72° W and 61° W. The weakening trend of the GS during the period from 1993 to 2016 is accompanied with a southward-shifting path, which is associated with the decline of the North Atlantic Oscillation (NAO) and possibly reduction in the Atlantic meridional overturning circulation (AMOC).

Keywords The Gulf Stream · Linear trends · North Atlantic Oscillation

1 Introduction

As the western boundary current of the Atlantic subtropical gyre and the upper branch of the Atlantic meridional overturning circulation (AMOC), the Gulf Stream (GS) transports a massive amount of heat northward to high latitudes, and thus plays an important role in the North Atlantic and European climate change (Rahmstorf 2002; Winton 2003; Rossby et al. 2014; McCarthy et al. 2015; Palter 2015). The GS contributes 20–30% to the total meridional heat transport of the global ocean and atmosphere at

26° N (Palter 2015 and references therein). An annual mean meridional heat transport of 1.33 PW (1 PW = 10¹⁵ W), including gyre and overturning heat transport components, was estimated by Johns et al. (2011) from the Rapid Climate-Meridional Overturning Circulation and Heatflux Array (RAPID-MOCHA) observing system along 26.5° N in the Atlantic during the period from April 2004 to October 2007. A recent analysis of the RAPID-MOCHA observations suggested that the annual average ocean heat transport decreased by 0.17 PW from 1.32 PW in 2004–2009 to 1.15 PW in 2009–2016 with a reduction of 2.5 Sv in the AMOC (Bryden et al. 2020). Change in heat transport carried by the GS causes the variability of the sea surface temperature (SST) in the North Atlantic (Delworth and Mann 2000; Latif et al. 2004; Rahmstorf et al. 2015). The GS is important for European climate by keeping some areas free of ice in the far North Atlantic and releasing sensible and latent heat to the atmosphere, which warms Europe downwind (Kaspi and Schneider 2011; Palter 2015; Yang et al. 2016).

The GS originates from the North Equatorial Current in the North Atlantic Ocean. It flows northward through the Straits of Florida and then along the North American east coast, supplied by recirculating gyres (Schmitz and McCartney 1993). At Cape Hatteras, the GS separates from the coast and turns to the east between the subtropical and subpolar gyres. After passing the Newfoundland Banks, it divides into two parts: one part flowing southeastward and the other turning northward. Much variability in the GS transport and pathway between the separation and the division has attracted many

This article is part of the Topical Collection on the *11th International Workshop on Modeling the Ocean (IWMO), Wuxi, China, 17–20 June 2019*

Responsible Editor: Tal Ezer

✉ Wen-Zhou Zhang
zwenzhou@xmu.edu.cn

✉ Fei Chai
fchai@sio.org.cn

- ¹ Fujian Provincial Key Laboratory for Coastal Ecology and Environmental Studies, Xiamen University, Xiamen, China
- ² State Key Laboratory of Satellite Ocean Environment Dynamics (Second Institute of Oceanography, SOA), Hangzhou, China
- ³ College of Ocean and Earth Sciences, Xiamen University, Xiamen, China
- ⁴ School of Marine Sciences, University of Maine, Orono, ME, USA
- ⁵ Princeton University, Princeton, NJ, USA

studies (e.g., Kelly et al. 1999; Rossby et al. 2005; Peña-Molino and Joyce 2008; Pérez-Hernández and Joyce 2014; Andres 2016). Kelly et al. (1999), using altimetric sea surface height (SSH) data, showed that evident seasonal variations appear in the surface transport and latitudinal position of the GS. Based on 11-year (1992–2003) acoustic Doppler current profiler current observations obtained along the Oleander transect between New Jersey and Bermuda, Rossby et al. (2005) analyzed the interannual variations in position and transport of the GS and found that the GS position is governed by the strength of circulation in the Slope Sea while the transport is driven by wind forcing. Peña-Molino and Joyce (2008) demonstrated that the latitudinal shift of the GS path is related to the change of properties in the Slope Water. Using gridded altimeter sea level anomaly weekly data from October 1992 to October 2012, Pérez-Hernández and Joyce (2014) investigated the variability of the GS path at several months to interannual time scales. Andres (2016) showed that the initiation position of GS meanders had strong interannual variability and a general westward shift during the period of 1993–2014, which increased both upper-ocean/deep-ocean and open-ocean/shelf interactions.

Substantial evidence from observations and model simulations indicates the decline of the AMOC in recent years (e.g., Weaver et al. 2012; Smeed et al. 2014, 2018; Ezer 2015; Caesar et al. 2018; Thornalley et al. 2018). Thirty independent climate models predicted a slowing down of the AMOC in the twenty-first century due to global warming (Weaver et al. 2012). An observing system of the Rapid Climate Change program designed to monitor the AMOC at 26.5° N observed a surprising decline ($-0.54 \text{ Sv year}^{-1}$) of the AMOC transport in its first 8.5 years (April 2004 to October 2012) of the deployment, much larger than the decline ($-0.05 \text{ Sv year}^{-1}$) in the twenty-first century predicted by climate models (Smeed et al. 2014; Srokosz and Bryden 2015). The observed AMOC has been in a reduced state since 2008 (Smeed et al. 2018). An AMOC index, based on SST observations in the subpolar gyre, revealed a long-term decline that suggests the AMOC has decreased by $3 \pm 1 \text{ Sv}$ (approximately 15%) since the 1950s (Caesar et al. 2018). From the SSH difference across the GS during 1935–2012, Ezer (2015) showed the decline in the long-term AMOC and the GS. Using a high-resolution climate model, Thomas et al. (2012) demonstrated that the reduction of the AMOC results from a reduced southward deep water flow and a reduced GS. The long-term trend of the GS transport has been debated in recent years. It has been observed that the transport of the Florida Current (a name used for the GS as it flows through the Straits of Florida) has a declining trend of $-0.29 \pm 0.23 \text{ Sv}$ per decade during the period of 1982–2017 (Blunden et al. 2018). Based on altimeter data, Ezer et al. (2013) showed that the GS between 70° W and 75.5° W has a significant weakening trend with a declining average SSH gradient across the GS since 2004. However,

no significant trend was found in the layer transport (at 52/55 m depth) of the GS derived from direct current observations along the Oleander transect over a 20-year period from 1992 to 2012 (Rossby et al. 2014). The study sites of both Ezer et al. (2013) and Rossby et al. (2014) are west of 65° W. Recently, Andres et al. (2020) compared the Oleander data with direct array measurements nearby and found large spatial variations in two GS sections separated by only 1.8° longitude, namely, the eastern one near 68.5° W shows decline and the western one at 70.3° W not. The large spatial and temporal variations were also discussed in Ezer (2019) who showed that large oscillations in GS transport and path with dominant periods of 2–5 years make it difficult to calculate long-term trends. Dong et al. (2019) demonstrated that the GS slowed down and shifted southward east of 65° W during the period of 1993–2016, based on temporally inhomogeneous all-satellite merged altimeter measurements.

Satellite altimeter data have been widely used to examine the variations of ocean circulations on various time scales (e.g., Kelly et al. 1999; Pérez-Hernández and Joyce 2014; Bisagni et al. 2017; Dong et al. 2019). Our detailed analyses, made on temporally homogenous two-satellite merged altimeter observations from 1993 to 2016, indicate that the surface maximum speed, transport, and meridional location of the GS have significant negative linear trends east of 61° W at the 95% level while they are small and not significant between 72° W and 61° W. The rest of this article is organized as follows. The data and methods used in this work are described in Section 2. The results about linear trends related to the GS are presented in Section 3. In Section 4, we discuss the dynamics which potentially induce these trends of the GS.

2 Data and methods

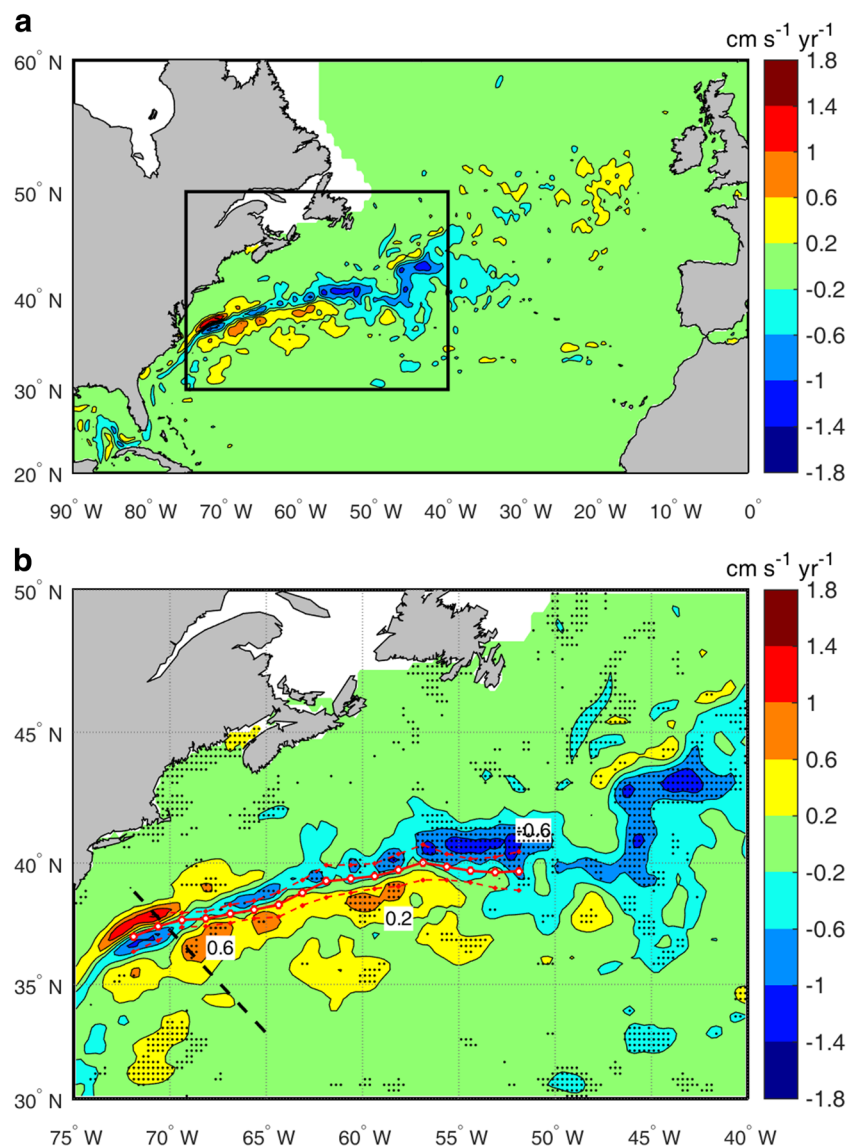
The daily SSH and surface geostrophic current and its anomaly data were derived from two-satellite (TOPEX/Poseidon (T/P) and ERS-1 or ERS-2, followed by Envisat and Jason-1 or Jason-2) merged altimeter observations by the Data Unification and Altimeter Combination System (DUACS). They were distributed by the Archiving, Validation and Interpretation of Satellites Oceanographic (AVISO) data and are now by the Copernicus Climate Change Service (C3S). As this dataset is obtained by two missions on the same two orbits, it is homogeneous and stable throughout the entire observation period, compared with the all-satellite merged dataset from all missions available (http://www.aviso.altimetry.fr/fileadmin/documents/data/tools/hdbk_duacs.pdf). Both the AVHRR satellite daily SST data (Reynolds et al. 2007) and the blended daily wind data (Zhang et al. 2006) were taken from the National Climatic Data Center (NCDC) of the National Oceanic and Atmospheric Administration

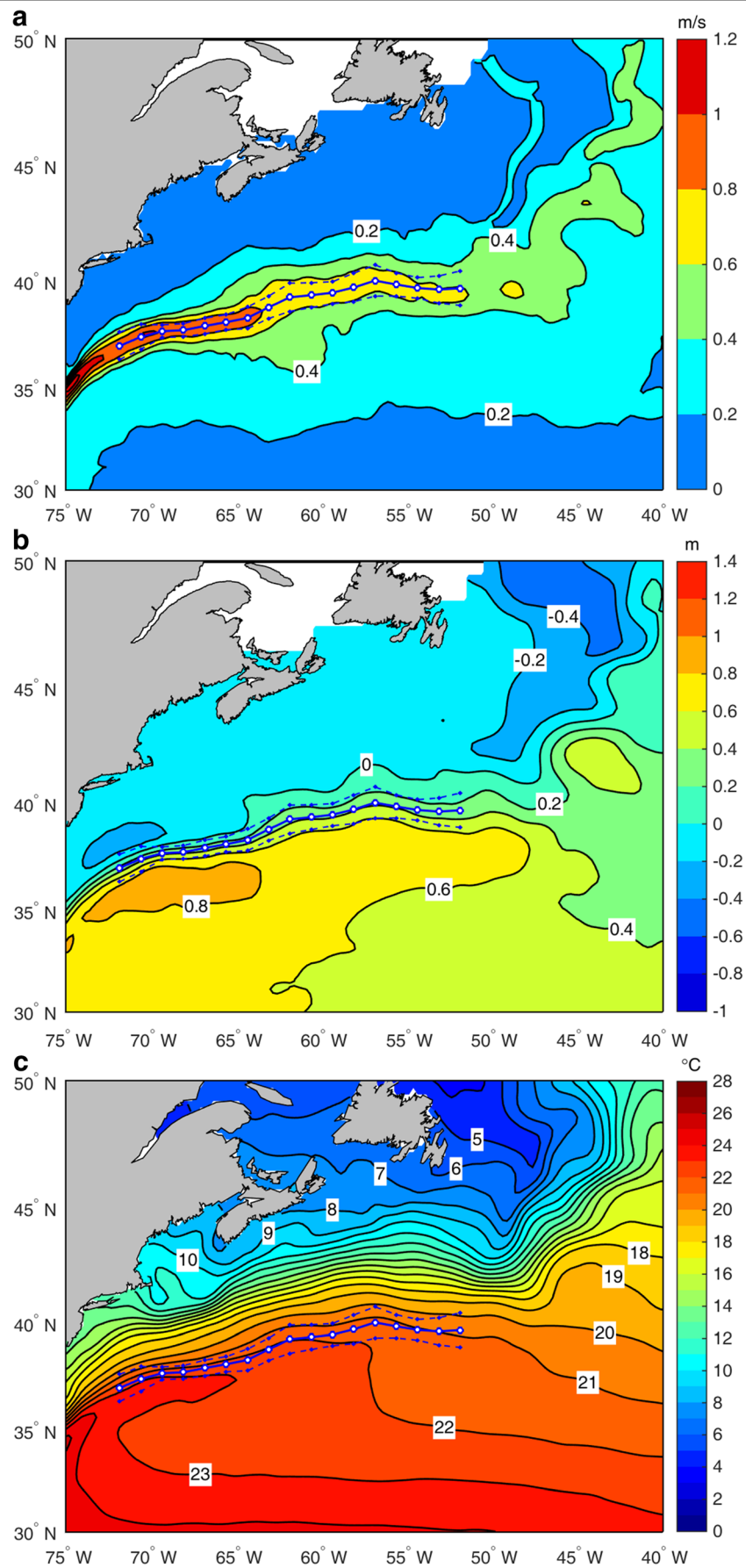
(NOAA). The monthly North Atlantic Oscillation (NAO) index data used to calculate the time series of annually averaged NAO were obtained from the Climate Prediction Center of the National Oceanic and Atmospheric Administration (<http://www.cpc.ncep.noaa.gov/products/precip/CWlink/pna/nao.shtml>).

Based on daily global absolute surface geostrophic currents, annual average velocity speed at each data grid was calculated year by year. Using these yearly velocity speed data, we obtained their linear trend at each grid point for the period of 1993–2016 (Fig. 1). To locate the path of the GS, 17 longitudes between 71.875° W and 51.875° W with a spacing of 1.25° were adopted to check the latitudinal locations of the GS, following Pérez-Hernández and Joyce (2014) who used 16 longitudes between 52° W and 72° W with an interval of 1.33°. At each longitude, the surface core location of the GS is

determined as follows: (1) between 35.5° N and 43.0° N the points at which the east component of surface geostrophic current is positive (toward east) are selected; (2) the latitude of the point with the maximum velocity speed among the selected points is taken as the corresponding surface core location of the GS. If there are more points than one having the maximum velocity speed, their mean latitude is the core location of the GS. The curve successively connecting all core locations depicts a daily path of the GS. During the period of interest, the time-averaged path is consistent with both the strongest mean velocity band and the greatest mean sea slope, located just at the south edge of the large SST gradient (Fig. 2). This path also coincides with the band of the largest standard deviation of sea level change in this region (not shown), in agreement with the GS path determined using the method of Pérez-Hernández and Joyce (2014). The maximum

Fig. 1 Map of surface geostrophic current speed trend during the period of 1993–2016. The interval of contours is 0.4 cm s^{-1} per year. In **b** (the zoomed-in area marked by a black rectangle in **a**), stippling marks regions where the trends are significant at the 95% confidence level. The red solid curve denotes the averaged GS path and red dashed curves show one standard deviation away from the averaged path. The black dashed line marks the Oleander route along which Rossby et al. (2010) obtained current observations





◀ **Fig. 2** The average GS path. The average GS path is separately superposed on the maps of **a** mean velocity speed, **b** mean SSH, and **c** mean SST during the period of 1993–2016

velocity speed was recorded at each core location along the GS daily path day by day. Then, we calculated the annual mean maximum velocity speed for each of 17 longitudes, simply averaged from the daily maximum velocity speed data without regard to their latitudinal location.

The daily SSH difference across the GS at each longitude mentioned previously was determined from daily SSH map by the maximum SSH south of the corresponding GS daily path minus the minimum north of the path in the region from 33° N to 43° N. Since this SSH difference was not obtained between two fixed sites, the meridional displacement of the GS path does not contaminate its value, and the GS broadening and narrowing is taken into account. Integrating geostrophic balance along a longitudinal section across the GS, we obtained

$$\begin{aligned} \Delta H &= \frac{f}{g} \int_{H_{\max}}^{H_{\min}} u_{gx}(y) dy = \frac{f}{g} \int_{H_{\max}}^{H_{\min}} u_g(s) \cos\theta \left(\frac{ds}{\cos\theta} \right) \\ &= \frac{f}{g} \int_{H_{\max}}^{H_{\min}} u_g(s) ds = \frac{f}{g} T_s, \end{aligned}$$

where ΔH is the SSH difference between the maximum SSH (H_{\max}) and the minimum SSH (H_{\min}) contours beside the GS path on a daily SSH map; f and g are the Coriolis parameter and the acceleration due to gravity, respectively; u_g is along-stream geostrophic current, normal to a cross-stream section (s) and u_{gx} is its eastward component normal to a longitudinal section (y), and θ is the angle between these two sections; the value of T_s is equal to that of the GS surface transport with 1 m depth near the surface at the longitude. Clearly, the SSH difference is in direct proportion to the surface transport. In other words, we can use this SSH difference to represent the GS surface transport in the geostrophic framework. Similar result has been given by Kelly et al. (1999) and Rossby et al. (2014). Annual average SSH difference was calculated from daily SSH differences. Based on altimeter data and in situ mooring observations from April 2010 to February 2013, Beal and Elipot (2016) found that sea surface height variance correlates well with the transport of the Agulhas Current at 34° S. Using an ocean model, Ezer (2001) has shown that the variations of sea level difference across the stream are coherent with those of the GS transport for time scales longer than 4–5 years. These suggest that the SSH difference can be taken as an index of the GS transport for long-term variations.

All trends presented in this paper are calculated by a linear regression method from annual average data with the autocorrelation time scale of 1 year. The 95% significance level was applied to the statistical inferences unless otherwise noted.

3 Results

3.1 The velocity speed trend in the GS region

In the trend map (Fig. 1) of surface geostrophic velocity speed derived from altimeter observations from 1993 to 2016, the most obvious feature is a band with negative values smaller than -0.2 cm s^{-1} per year. Its shape and location coincide with the GS. Figure 1b shows that the averaged path of the GS aligns with the band of negative trend in velocity speed, but deviates slightly from the negative trend centers. The negative center west of 69° W is to the south of the path, while that east of 69° W is to the north of the path. The decline of velocity speed in the GS region may be caused by two factors: weakening of the GS and/or meridional displacement of its path.

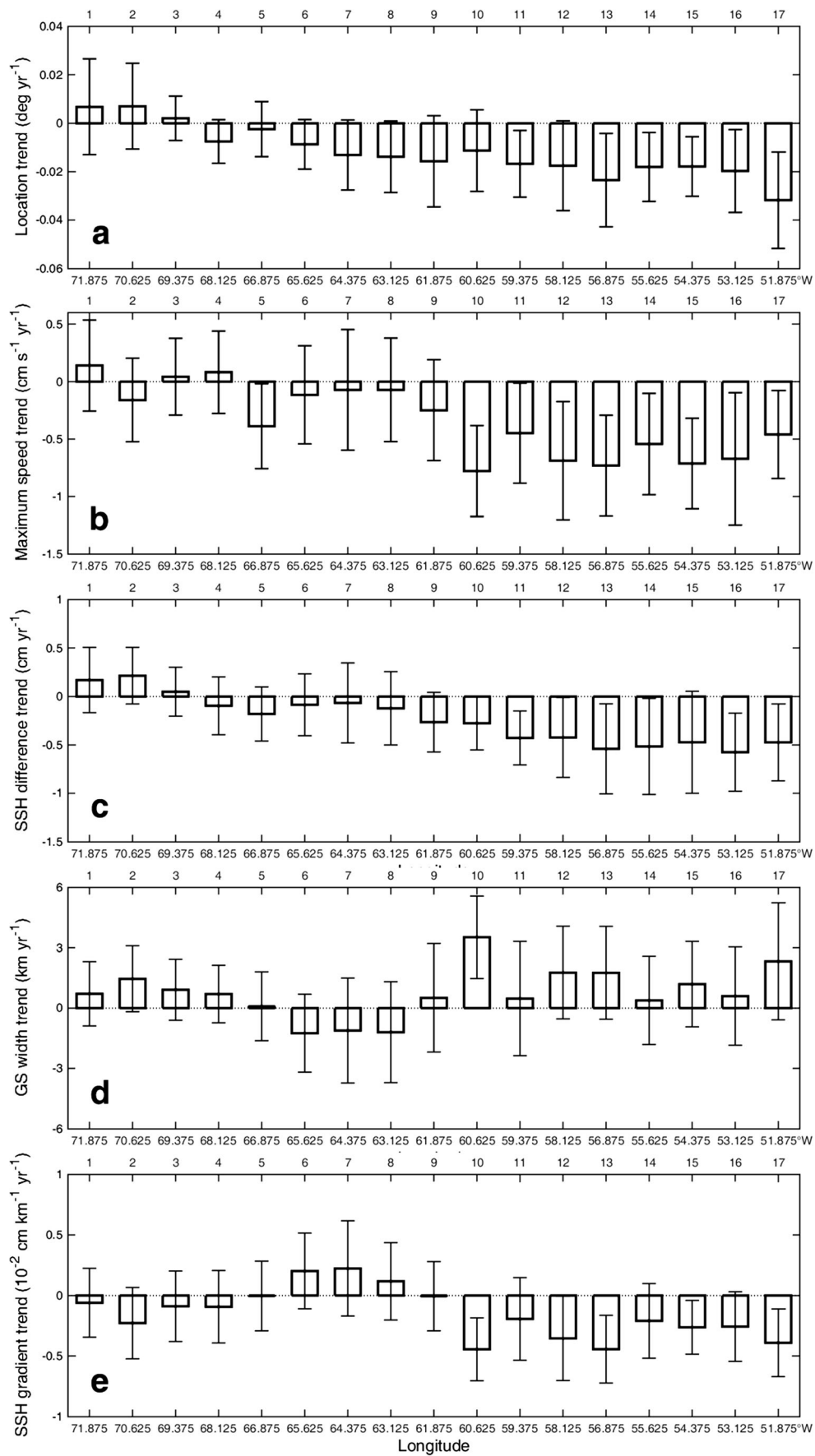
3.2 Meridional displacement of the GS path

Figure 3a shows that during the period of 1993–2016, the GS path had a negative (southward) trend east of 69° W, which is significant east of 58° W. The southward displacement trend was in the range of -0.002 – 0.032° (approximately 0.3–3.5 km) per year, with a mean of 1.7 km per year. West of 69° W, the trend was positive (northward), though not significant. The above results are in good agreement with the trend of the GS North Wall (GSNW) position during the period of 1993–2013, estimated by Bisagni et al. (2017). They showed that the GSNW had a southward trend at 55°, 60°, 65°, and 70° W, but only that at 55° W was significant with the 95% confidence level.

Meridional displacement or shift of the GS path usually influences the change of current at a fixed point near the GS: southward (northward) displacement tends to weaken the current in the north (south) and strengthen the current in the south (north). As a result, the long-term trend of the GS path displacement is anticipated to induce a corresponding trend in velocity. The negative velocity speed trend center occurred to the north (south) of the time-averaged path east (west) of 69° W, where the GS path has a southward (northward) displacement trend; meanwhile, the positive velocity speed trend appeared on the opposite side (Figs. 1b and 3a). The above pattern suggests that the trend of Eulerian velocity speed in this region is partly caused by the long-term meridional displacement of the GS path.

3.3 Weakening of the GS

The annual mean maximum velocity speed has a significant negative trend east of 61° W (Fig. 3b). The negative trend is in the range of -0.45 to -0.78 cm s^{-1} per year. West of 61° W, the maximum velocity speed trend changes from negative to positive further upstream, but most values are not significantly different from zero in terms of the 95% significance level.



◀ **Fig. 3** Trends of **a** latitudinal location (deg year^{-1}), **b** maximum speed ($\text{cm s}^{-1} \text{year}^{-1}$), **c** SSH difference (cm year^{-1}), **d** width (km year^{-1}), and **e** cross-stream mean SSH gradient ($10^{-2} \text{cm km}^{-1} \text{year}^{-1}$) of the GS at each labelled longitude during the period of 1993–2016. Northward (southward) displacement of the GS path is positive (negative) in **a**. Each error bar denotes the corresponding 95% confidence interval

Similar to the maximum velocity speed, the annual mean SSH difference declines significantly east of 61°W , while this negative trend lessens westward and even becomes positive, but not significant, west of 69°W (Fig. 3c). With respect to the corresponding mean SSH difference (1.05–1.15 m) at each longitude, the trend of -0.28 to $-0.58 \text{ cm year}^{-1}$ at the downstream east of 61°W means that the GS surface transport might have declined 5.8–13.0% during the last 24 years (0.24–0.54% per year).

Taking the direction of the maximum velocity as the GS flowing direction, we obtained the width and mean SSH gradient of each cross-stream section at the above-mentioned longitudes. The GS broadened with weakening SSH gradient east of 62°W and west of 66°W during the period from 1993 to 2016 while it narrowed with intensifying SSH gradient in between (Fig. 3d, e). The mean SSH gradients across the GS east of 61°W have similar reducing trends to the corresponding SSH differences although some of them are not significant due to the low confidence of the GS width trends.

4 Discussion and conclusion

Both the surface velocity speed and the SSH difference (Figs. 1 and 3) indicate that the GS has declined noticeably downstream east of 61°W in the past 24 years, whereas it is not significant upstream. Rossby et al. (2010) found no significant trend in the GS transport between 68°W and 71°W (marked by a black dashed line in Fig. 1b) using directly measured near-surface currents during the period of 1993–2009. Later, Rossby et al. (2014) obtained a trend of -0.13% per year for the GS layer transport (obtained by integrating downstream velocity along a cross-stream section) at the same place during the longer period of 1993–2012. However, the trend is not significantly different from zero at the 95% confidence level. The more recent analysis of Andres et al. (2020) did show a clearer downward trend in the GS transport just east of the Oleander line (see their Fig. 10). Andres et al. (2020) suggested that the mean GS transport at 68.5°W during 2010–2014 is about 10% weaker than that observed by a moored array of the same area in the late 1980s. Given the place where they observed the GS transport, their results are qualitatively in agreement with ours west of 61°W (Fig. 3a, c). Our result obtained from continuous two-satellite merged altimeter observations during 1993–2016 demonstrates that the

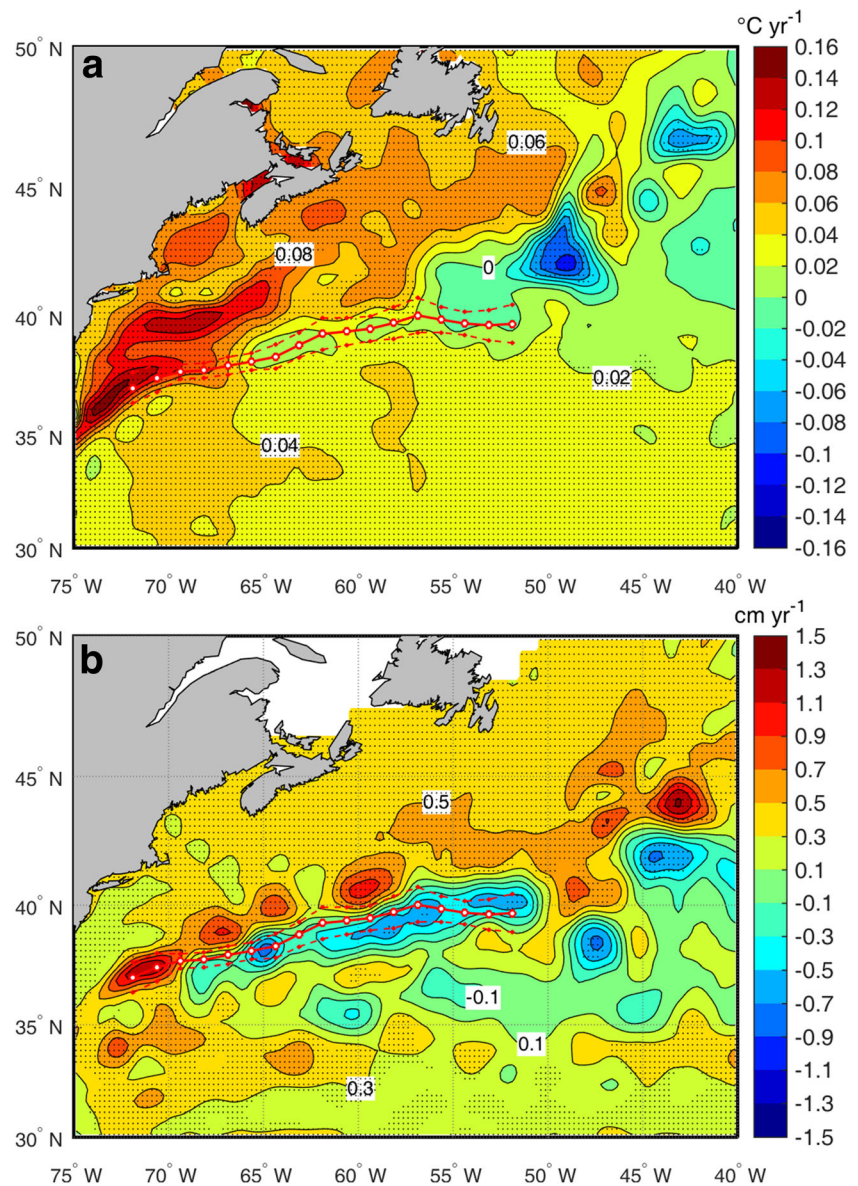
weakening and southward displacement trends of the GS occur in the region east of 69°W and they are significant only east of 61°W (Fig. 3). Using all-satellite merged altimeter data during the same period, Dong et al. (2019) presented a similar result that the GS has a weakening trend east of 65°W , accompanied with a southward-shifting path.

Heat advection and divergence due to ocean currents play an important role in the change and pattern of SST (Curry and McCartney 2001; McCarthy et al. 2015). An obvious cooling with a negative trend of 0 to $-0.12 \text{ }^\circ\text{C year}^{-1}$ in the SST occurs in the region just northeast of the GS (Fig. 4a), which may be associated with the weakening of the GS. Figure 4b shows that a positive trend ($0.3\text{--}1.1 \text{ cm year}^{-1}$) of SSH occurs in the northwest of the GS, while a negative one ($-0.1\text{--}0.7 \text{ cm year}^{-1}$) occurs in the southeast, indicating a reduction of sea level gradient across the GS. It is obvious that positive SST and SSH anomalies appear in the area between the coast and the GS east of 72°W (Fig. 4). The warming sea and elevated SSH along the coast due to the weakening GS have been an area of great concern and research on coastal sea level rise along the US East Coast (Ezer et al. 2013; Ezer 2019). In a narrow central band along the averaged GS path, the negative (positive) SSH trend east (west) of 69°W partly relates to the southward (northward) displacement of the GS path (Fig. 4b). These support the weakening and southward displacement of the GS (at least its surface part) downstream over the past 24 years.

Yang et al. (2016) found that the western boundary currents except the GS are intensifying and shifting poleward due to the long-term effects of global warming. They suggested that the intensification and poleward shift of near-surface ocean winds dynamically cause this change. However, Beal and Elipot (2016) showed that Agulhas Current (a western boundary current in the Indian Ocean) has broadened with a stable total transport, not intensified in its mean flow, since the early 1990s as a result of increasing eddy activity. Seen from surface signals east of 61°W presented in this work, the GS actually behaved much differently from other western boundary currents from 1993 to 2016. Despite the intensifying and poleward-shifting zonal winds over the North Atlantic (Yang et al. 2016), the GS significantly weakened in surface transport and velocity speed and displaced southward (Figs. 1 and 3), rather than intensified and shifted northward. It had a negative surface transport trend without a significant broadening (Fig. 3). These discrepancies are quite likely because the GS is connected to the AMOC under the influence of the NAO, as is discussed below.

The slowing down of the GS during the past 24 years may be attributed to the weakening of the AMOC and the NAO. Observations from 2004 to 2017 suggested that the AMOC has a downward trend since 2004 (Smeed et al. 2014) and has been in a reduced state since 2008 (Smeed et al. 2018). The northward ocean heat transport analysis also indicated that a

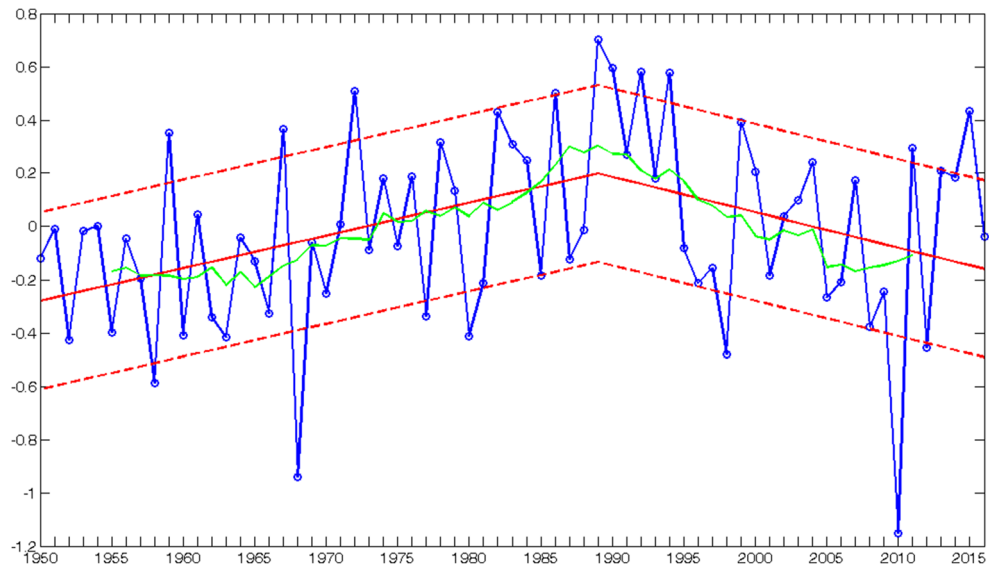
Fig. 4 Trends of the annual mean SST and SSH. Contour intervals are $0.02\text{ }^{\circ}\text{C yr}^{-1}$ and 0.2 cm yr^{-1} for the **a** SST and **b** SSH, respectively. The annual mean SST was averaged from the Advanced Very High Resolution Radiometer (AVHRR) satellite daily SST data. Areas where the significance level of the trends is above 95% are stippled



reduction of 0.17 PW in ocean heat transport corresponds to a drop of 2.5 Sv in the AMOC during 2009–2016, compared with the values during 2004–2009 (Bryden et al. 2020). Ezer (2015) found that the Oleander total transport is highly correlated with the AMOC during 2004–2012. As one component of internally fluctuating Atlantic circulations, the GS transport and flow path adjust to the evolution of thermohaline (density-driven) circulation and wind-driven circulation at interannual and longer time scales. This adjustment is directly or indirectly linked to external atmospheric forcing, since the changes of the thermohaline and wind-driven circulations are mainly controlled by atmospheric forcing via buoyancy flux (freshwater and heat fluxes) and momentum flux (wind stress) (Delworth and Greatbatch 2000; Curry and McCartney 2001; Eden and Jung 2001; Rahmstorf et al. 2015; Thornalley et al. 2018). The NAO is the principal mode in the variability of the surface

atmospheric circulation in the Atlantic and a major driver of its interannual and longer variability (Hurrell 1995; Taylor and Stephens 1998). An index based on the difference of normalized pressures between Lisbon, Portugal, and Stykkisholmur, Iceland, describes the variability of the NAO (Hurrell 1995), reflecting the strength of middle latitude westerlies and changes of heat, freshwater, and momentum fluxes in the North Atlantic (Curry and McCartney 2001). The North Atlantic Deep Water is formed in the Labrador Sea and in the Nordic Seas via convection related to the NAO. The Labrador Sea convection has a dominant influence on the variability of the AMOC, with a significantly positive correlation between them (Medhaug et al. 2012). During the negative phase of the NAO index, a reduced convection in the Labrador Sea, due to decreased heat loss, more precipitation, and weaker wind, corresponds to a weaker AMOC, and the situation is

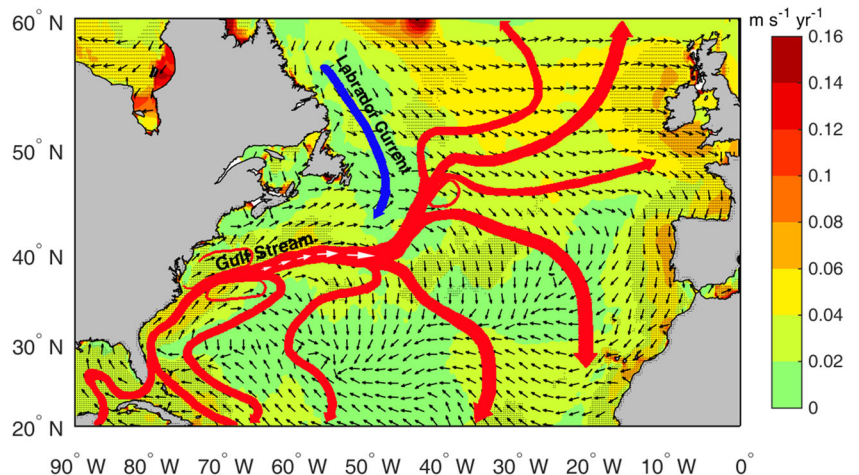
Fig. 5 Variability of the NAO. Red lines denote the linear regression trend with one standard derivation (dashed line) away from the corresponding trend. The green curve shows the 5-year running average



reversed during the positive phase (Medhaug et al. 2012). Meanwhile, the subpolar and subtropical gyre circulations are weakened (intensified) for a low (high) NAO index (Curry and McCartney 2001), and the boundary between the two gyres is more (less) zonal (Lohmann et al. 2009). The annual averaged NAO index reached its maximum value in 1989 during the record period of 1950–2016. Subsequently, the NAO index had a significant declining trend at the level of 95% (Fig. 5). The weakening of the GS, with a southward-displaced path east of 69° W during 1993–2016, is associated with the decline of the NAO according to previous studies (e.g., Taylor and Stephens 1998; Curry and McCartney 2001; Chaudhuri et al. 2011). Using a transport index representing the upper 2000-db eastward baroclinic mass transport, Curry and McCartney (2001) demonstrated that the GS gradually weakened during the 1960s, with low NAO, and then strengthened in the subsequent 25 years with high NAO. Numerical model results by Chaudhuri et al.

(2011) indicated that the GS transport, downstream of Cape Hatteras, is enhanced during a positive NAO phase, while it is reduced during a negative NAO phase. Note that there are large interannual and decadal variations in the NAO and in particular the most extreme decline in 2010 (Fig. 5), which probably largely contributes to the downward linear trend after the 1990s. The extreme NAO decline corresponds to the 30% reduction of the AMOC, resulting in an anomalously high sea level along the Northeast Coast of North America (Ezer 2015; Goddard et al. 2015). This indicates that they (NAO, AMOC, and sea level) are connected to each other. Dong et al. (2019) suggested that the slowdown of the GS is largely caused by the SSH increase due to regional ocean warming (thermal expansion) and mass augment to the north of the GS. The link between the NAO and the SSH change across the GS is related to complicated hydrodynamic adjustments and thermodynamic processes, which is still not clear to date.

Fig. 6 Schematic map of the GS system superposed on wind trends. Shading and black arrows denote the magnitude (m s^{-1} per year) and direction of wind trend vectors, respectively, during the period of 1993–2016. The length of the white arrows qualitatively describes the reduction magnitude of the GS transport, according to Fig. 2c



The southward path displacement coincides with the slowdown of the GS (Fig. 3). Both model simulations and observations have indicated that a strong (weak) GS transport usually accompanies with a northerly (southerly) path (Curry and McCartney 2001; De Coëtlogon et al. 2006; Ezer et al. 2013). The GS separation from the North American coast and its path downstream of Cape Hatteras shift meridionally with variations of the northern recirculation gyre (NRG), the southward-flowing Labrador Current (LC), the deep western boundary current (DWBC), and the AMOC related to the NAO (Rossby and Benway 2000; De Coëtlogon et al. 2006; Joyce and Zhang 2010; Ezer et al. 2013; Pérez-Hernández and Joyce 2014; Bisagni et al. 2017). A high (low) NAO index accompanied by strong (weak) westerly and trade winds is favorable for northward (southward) displacement of the GS path obtained from monthly charts of the GSNW (Taylor and Stephens 1998). Independent observations (Frankignoul et al. 2001) and model results (De Coëtlogon et al. 2006) also supported this relationship between the GS path and the NAO.

From the trends (as shown in Fig. 3), the GS behaved differently at the upstream (west of 69° W) and at the downstream (east of 69° W), not only in its meridional displacement but also in its surface transport. At the upstream, the GS exhibited trends, i.e., enhanced surface transport and a northward-displaced path, opposite to the corresponding trends at the downstream (Fig. 3). This spatial result is consistent with the findings of Dong et al. (2019) and Andres et al. (2020). The longitude of 69° W fortuitously separated the two GS sections analyzed by Andres et al. (2020) where the GS had different change trends as mentioned previously. The magnitudes of both surface transport and displacement trends west of 69° W are smaller and insignificant, compared with those east of 61° W (Fig. 3). Previous studies have shown that the GS exhibits different behaviors in meridional displacement along its path after the separation at Cape Hatteras (Gangopadhyay et al. 2016; Bisagni et al. 2017; Dong et al. 2019; Andres et al. 2020). The magnitude of variability in the GSNW position decreased westward between 55° W and 70° W, during the period of 1993–2013 (Bisagni et al. 2017). In the frequency domain, a significant near-decadal frequency, with a longer period of ~ 10 years, occurs west of 65° W, but a dominant interannual one, with a shorter period of ~ 5 years, occurs east of 60° W (Gangopadhyay et al. 2016; Bisagni et al. 2017). The above near-decadal and interannual signals are absent or negligible in the regions east of 60° W and west of 70° W, respectively (Gangopadhyay et al. 2016). These two frequencies both appear in the spectrum of the NAO time series. The near-decadal signal is due to integrated basinwide wind effects, the DWBC, and northern and

southern recirculation gyres, while the interannual signal is mainly linked to the southward-flowing LC (Gangopadhyay et al. 2016; Bisagni et al. 2017). Andres et al. (2020) demonstrated that near 70.3° W the intensified anticyclonic flank south of the GS and the weakened cyclonic flank north of the GS cause little temporal change in the across-stream SSH difference and upper-ocean transport while near 68.5° W the weakened cyclonic flank alone has no such effect. Dong et al. (2019) reckoned that the SSH changes north of the GS largely determine the variations of SSH difference across the stream east of 65° W whereas the SSH changes south of the GS are dominant west of 70° W, suggesting that different mechanisms control the cross-stream SSH difference in the eastern and western portions of the GS. Additionally, an anticyclonic pattern in wind trend occurs in the southwestern North Atlantic (Fig. 6), which may enhance Ekman transport and recirculation in the upstream region of the GS. These processes (large-scale wind patterns, the DWBC, the recirculation gyres, the southward-flowing LC) in response to the NAO impose different effects on different GS segments, which are responsible for non-uniform behavior of the GS along its path. The diverse trends of the GS reflect the combined functions of these processes at longer time scales.

The temporal length of the remote sensing data is not sufficient to identify whether the change trends of the GS presented here are part of its multi-decadal variations, long-term trends, or their combination. Nevertheless, substantial attention should be paid to the potential impacts related to the slowing down of the GS. These impacts include a higher sea level rising rate and more flooding along the east coast of the USA, cooling in the North Atlantic, and a cold and dry climate in northern Europe, most of which have been reflected in observations (Ezer et al. 2013; Palter 2015). More observations are required in the GS region, especially east of 69° W, for further investigation on the variability of the GS and relevant impacts.

Acknowledgments This study is a contribution to the international IMBER project. The daily SSH and surface geostrophic current and its anomaly data were obtained from the Archiving, Validation and Interpretation of Satellites Oceanographic (AVISO) data project (<ftp://ftp.aviso.oceanobs.com/>), and both the AVHRR satellite daily SST data and the blended (multi-satellite wind speed observations and wind directions from the NCEP Reanalysis 2) daily wind data were from the National Climatic Data Center (NCDC) of the National Oceanic and Atmospheric Administration (NOAA) (<http://www.ncdc.noaa.gov/>). The monthly North Atlantic Oscillation (NAO) index data were downloaded from the website of the Climate Prediction Center of the National Oceanic and Atmospheric Administration (<http://www.cpc.ncep.noaa.gov/products/precip/CWlink/pna/nao.shtml>).

Funding information This work was jointly supported by the State Key R&D project (2016YFA0601103) and the National Natural Science Foundation of China (41776015).

References

- Andres M (2016) On the recent destabilization of the Gulf Stream path downstream of Cape Hatteras. *Geophys Res Lett* 43:9836–9842
- Andres M, Donohue KA, Toole JM (2020) The Gulf Stream's path and time-averaged velocity structure and transport at 68.5°W and 70.3°W. *Deep-Sea Res I Oceanogr Res Pap* 156:103179
- Beal LM, Elipot S (2016) Broadening not strengthening of the Agulhas Current since the early 1990s. *Nature* 540:570–573
- Bisagni JJ, Gangopadhyay A, Sanchez-Franks A (2017) Secular change and inter-annual variability of the Gulf Stream position, 1993–2013, 70°–55°W. *Deep-Sea Res I Oceanogr Res Pap* 125:1–10
- Blunden J, Arndt DS, Hartfield G (2018) State of the climate in 2017. *Bull Am Meteorol Soc* 99(8):Si–S310
- Bryden HL, Johns WE, King BA, McCarthy G, McDonagh EL, Moat BI, Smeed DA (2020) Reduction in ocean heat transport at 26°N since 2008 cools the eastern subpolar gyre of the North Atlantic Ocean. *J Clim* 33:1677–1689
- Caesar L, Rahmstorf S, Robinson A, Feulner G, Saba V (2018) Observed fingerprint of a weakening Atlantic Ocean overturning circulation. *Nature* 556:191–196
- Chaudhuri AH, Gangopadhyay A, Bisagni JJ (2011) Response of the Gulf Stream transport to characteristic high and low phases of the North Atlantic Oscillation. *Ocean Model* 39:220–232
- Curry RG, McCartney MS (2001) Ocean gyre circulation changes associated with the North Atlantic Oscillation. *J Phys Oceanogr* 31:3374–3400
- De Coëtlogon G, Frankignoul C, Bentsen M, Delon C, Haak H, Masina S, Pardaens A (2006) Gulf Stream variability in five oceanic general circulation models. *J Phys Oceanogr* 36:2119–2135
- Delworth TL, Greatbatch RJ (2000) Multidecadal thermohaline circulation variability driven by atmospheric surface flux forcing. *J Clim* 13:1481–1495
- Delworth TL, Mann ME (2000) Observed and simulated multidecadal variability in the Northern Hemisphere. *Clim Dyn* 16:661–676
- Dong S, Baringer MO, Goni GJ (2019) Slow down of the Gulf Stream during 1993–2016. *Sci Rep* 9:6672
- Eden C, Jung T (2001) North Atlantic interdecadal variability: oceanic response to the North Atlantic Oscillation (1865–1997). *J Clim* 14:676–691
- Ezer T (2001) Can long-term variability in the Gulf Stream transport be inferred from sea level? *Geophys Res Lett* 28:1031–1034
- Ezer T (2015) Detecting changes in the transport of the Gulf Stream and the Atlantic overturning circulation from coastal sea level data: the extreme decline in 2009–2010 and estimated variations for 1935–2012. *Glob Planet Chang* 129:23–36
- Ezer T (2019) Regional differences in sea level rise between the Mid-Atlantic Bight and the South Atlantic Bight: is the Gulf Stream to blame? *Earth's Future* 7(7):771–783
- Ezer T, Atkinson LP, Corlett WB, Blanco JL (2013) Gulf Stream's induced sea level rise and variability along the U.S. mid-Atlantic coast. *J Geophys Res Oceans* 118:685–697
- Frankignoul C, De Coëtlogon G, Joyce TJ, Dong S (2001) Gulf Stream variability and ocean–atmosphere interactions. *J Phys Oceanogr* 31:3516–3529
- Gangopadhyay A, Chaudhuri AH, Taylor AH (2016) On the nature of temporal variability of the Gulf Stream path from 75° to 55°W. *Earth Interact* 20(9):1–17
- Goddard PB, Yin J, Griffies SM, Zhang S (2015) An extreme event of sea-level rise along the Northeast Coast of North America in 2009–2010. *Nat Commun* 6:6345
- Hurrell JW (1995) Decadal trends in the North Atlantic Oscillation: regional temperatures and precipitation. *Science* 269:676–679
- Johns WE, Baringer MO, Beal LM, Cunningham SA, Kanzow T, Bryden HL, Hirschi JJM, Marotzke J, Meinen CS, Shaw B, Curry R (2011) Continuous, array-based estimates of Atlantic Ocean heat transport at 26.5°N. *J Clim* 24:2429–2449
- Joyce TM, Zhang R (2010) On the path of the Gulf Stream and the Atlantic meridional overturning circulation. *J Clim* 23:3146–3154
- Kaspi Y, Schneider T (2011) Winter cold of eastern continental boundaries induced by warm ocean waters. *Nature* 471:621–624
- Kelly KA, Singh S, Huang RX (1999) Seasonal variations of sea surface height in the Gulf Stream region. *J Phys Oceanogr* 29:313–327
- Latif M, Roeckner E, Botzet M, Esch M, Haak H, Hagemann S, Jungclaus J, Legutke S, Marsland S, Mikolajewicz U, Mitchell J (2004) Reconstructing, monitoring, and predicting multidecadal-scale changes in the North Atlantic thermohaline circulation with sea surface temperature. *J Clim* 17:1605–1614
- Lohmann K, Drange H, Bentsen M (2009) Response of the North Atlantic subpolar gyre to persistent North Atlantic oscillation like forcing. *Clim Dyn* 32:273–285
- McCarthy GD, Haigh ID, Hirschi JJM, Grist JP, Smeed DA (2015) Ocean impact on decadal Atlantic climate variability revealed by sea-level observations. *Nature* 521:508–510
- Medhaug I, Langehaug HR, Eldevik T, Furevik T, Bentsen M (2012) Mechanisms for decadal scale variability in a simulated Atlantic meridional overturning circulation. *Clim Dyn* 39:77–93
- Palter JB (2015) The role of the Gulf Stream in European climate. *Annu Rev Mar Sci* 7:113–137
- Peña-Molino B, Joyce TM (2008) Variability in the Slope Water and its relation to the Gulf Stream path. *Geophys Res Lett* 35:L03606
- Pérez-Hernández MD, Joyce TM (2014) Two modes of Gulf Stream variability revealed in the last two decades of satellite altimeter data. *J Phys Oceanogr* 44:149–163
- Rahmstorf S (2002) Ocean circulation and climate during the past 120,000 years. *Nature* 419:207–214
- Rahmstorf S, Box JE, Feulner G, Mann ME, Robinson A, Rutherford S, Schaffernicht EJ (2015) Exceptional twentieth-century slowdown in Atlantic Ocean overturning circulation. *Nat Clim Chang* 5:475–480
- Reynolds RW, Smith TM, Liu C, Chelton DB, Casey KS, Schlax MG (2007) Daily high-resolution-blended analyses for sea surface temperature. *J Clim* 20:5473–5496
- Rosby T, Benway RL (2000) Slow variations in mean path of the Gulf Stream east of Cape Hatteras. *Geophys Res Lett* 27:117–120
- Rosby T, Flagg C, Donohue K (2005) Interannual variations in upper-ocean transport by the Gulf Stream and adjacent waters between New Jersey and Bermuda. *J Mar Res* 63:203–226
- Rosby T, Flagg C, Donohue K (2010) On the variability of Gulf Stream transport from seasonal to decadal timescales. *J Mar Res* 68:503–522
- Rosby T, Flagg CN, Donohue K, Sanchez-Franks A, Lillibridge J (2014) On the long-term stability of Gulf Stream transport based on 20 years of direct measurements. *Geophys Res Lett* 41:114–120
- Schmitz WJ, McCartney MS (1993) On the North Atlantic circulation. *Rev Geophys* 31:29–49
- Smeed DA, McCarthy GD, Cunningham SA, Frajka-Williams E, Rayner D, Johns WE, Meinen CS, Baringer MO, Moat BI, Duchez A, Bryden HL (2014) Observed decline of the Atlantic meridional overturning circulation 2004–2012. *Ocean Sci* 10:29–38
- Smeed DA, Josey SA, Beaulieu C, Johns WE, Moat BI, Frajka-Williams E, Rayner D, Meinen CS, Baringer MO, Bryden HL, McCarthy GD (2018) The North Atlantic Ocean is in a state of reduced overturning. *Geophys Res Lett* 45:1527–1533
- Srokosz MA, Bryden HL (2015) Observing the Atlantic meridional overturning circulation yields a decade of inevitable surprises. *Science* 348(6241):1255575
- Taylor AH, Stephens JA (1998) The North Atlantic Oscillation and the latitude of the Gulf Stream. *Tellus* 50A:134–142
- Thomas MD, De Boer AM, Stevens DP, Johnson HL (2012) Upper ocean manifestations of a reducing meridional overturning circulation. *Geophys Res Lett* 39:L16609

- Thornalley DJR, Oppo DW, Ortega P, Robson JI, Brierley CM, Davis R, Hall IR, Moffa-Sanchez P, Rose NL, Spooner PT, Yashayaev I, Keigwin LD (2018) Anomalously weak Labrador Sea convection and Atlantic overturning during the past 150 years. *Nature* 556:227–230
- Weaver AJ, Sedláček J, Eby M, Alexander K, Cresspin E, Fichefet T, Philippon-Berthier G, Joos F, Kawamiya M, Matsumoto K, Steinacher M, Tachiiri K, Tokos K, Yoshimori M, Zickfeld K (2012) Stability of the Atlantic meridional overturning circulation: a model intercomparison. *Geophys Res Lett* 39:L20709
- Winton M (2003) On the climatic impact of ocean circulation. *J Clim* 16: 2875–2889
- Yang H, Lohmann G, Wei W, Dima M, Ionita M, Liu J (2016) Intensification and poleward shift of subtropical western boundary currents in a warming climate. *J Geophys Res Oceans* 121:4928–4945
- Zhang HM, Bates JJ, Reynolds RW (2006) Assessment of composite global sampling: sea surface wind speed. *Geophys Res Lett* 33: L17714